Water Resources Management (2022) 36:5371–5399
https://doi.org/10.1007/s11269-022-03313-y

Changing Pattern of Intensity–Duration–Frequency Relationship of Precipitation due to Climate Change

Subhra Sekhar Maity[1] · Rajib Maity[1]

Received: 5 October 2021 / Accepted: 26 August 2022 / Published online: 28 September 2022

Abstract

Intensification of hydrologic cycle, and consequence rise of intense short-term precipitation, are considered as the manifestations of climate change. This may lead to an alteration in Intensity–Duration–Frequency (IDF) relationship that may change other hydrological processes as well. The IDF relationship also serves as a crucial information for the design of any water infrastructure. This study investigates the spatiotemporal changes in IDF relationship involving hourly precipitation events between past and future climate at various return periods across India that spans over a wide range of climatology. Contrast between historical (1979–2014), using two reanalysis data, and future periods (immediate future: 2015–2039, near-future: 2040–2059 and far-future: 2060–2100) is explored along with its spatial (re-) distribution. The future simulations of precipitation are derived from three climate models, participating in 6th phase of Coupled Model Intercomparison Project (CMIP6), for three shared socio-economic pathways (SSPs), i.e., SSP126, SSP245 and SSP585. The results show that almost entire Indian mainland will experience an increase (~41–44%) in the hourly precipitation intensity under the worst climate change scenario (SSP585) with a return period as low as 2 years (almost a regular incidence). Furthermore, even under a moderate climate change scenario (SSP245), almost entire Indian mainland (~82–99% of spatial extent) will be affected from a significant increase (on an average 19%) in the hourly precipitation intensity. It is true for higher return periods as well. Findings of the study are alarming for many water infrastructures. This study develops new set of IDF curves across India considering a changing climate that will be useful to set a revised design criteria for water infrastructure.

Keywords Climate change · Precipitation · Intensity · Duration · Frequency · IDF relationship

1 Introduction

Intensity-Duration-Frequency (IDF) curves provide a quantitative relationship between precipitation intensity over several durations and frequencies (return levels or return periods). This information is crucial for the design of water infrastructures, and if there is any alteration, it is profound consequences on other hydrological processes. Conventionally, estimation

✉ Rajib Maity
rajib@civil.iitkgp.ac.in

[1] Department of Civil Engineering, Indian Institute of Technology Kharagpur, Kharagpur 721302, West Bengal, India

of IDF curves is based on historical data. However, due to the changing climate, the precipitation characteristics change from the past (historical period) to future, since the extreme precipitation events are intensifying globally as a manifestation of climate change (Roy and Balling 2004; Semmler and Jacob 2004; Arnbjerg-Nielsen 2012; Asadieh and Krakauer 2015). Extreme precipitation has increased at roughly two-thirds of the stations, and the percentage of stations with significantly increasing trends is significantly high for the entire globe (Sun et al. 2021) and it is also observed that short-duration extreme precipitation intensity can respond more strongly to global warming compared to daily extremes (Fowler et al. 2021). Historically, extreme precipitation events caused heavy damages to infrastructures (Keller and Atzl 2014; Liu et al. 2021), and further intensification due to climate change poses a major challenge to the designers. In the past decade, several incidences of extreme precipitation led to severe floods across India, e.g., Uttarakhand, Srinagar, Chennai, Gujarat (Ray et al. 2019), Kerala (Mishra and Shah 2018). The damages to the infrastructure and severity of the flooding events indicate the inadequacy of existing hydraulic structures to withstand the changing climate. In practice, hydraulic structures such as culverts, stormwater drainage, bridges, small dams, and regional flood protection works such as levees, highway drainage etc. are designed using IDF relationships, which relate the intensity of precipitation with its return period and duration (Kang et al. 2009; Bhatkoti et al. 2016; Bertini et al. 2020). Traditionally, the IDF curves are constructed based on sufficiently long historical precipitation records, which may not reflect the temporal change due to climate change. So, in order to investigate the future changes in IDF curves, researchers have used outputs from climates models - General Circulation Models (GCM) or Regional Climate Models (RCM) or a combination thereof. These models incorporate the effect of climate change by considering different warming and socio-economic scenarios. On the basis of the future simulations, several studies have shown an increase in intensity of precipitation throughout the globe. For instance, future simulations from Canadian Regional Climate Model (CRCM) indicated a decrease in return periods for 2- and 6-h duration precipitation by half and by one-third for 12- and 24-h events over the Southern Quebec region in Canada (Mailhot et al. 2007). Coordinated Downscaling Experiment (CORDEX) simulation over Europe showed a 16–27% increase of IDF ordinates for different return periods (Hosseinzadehtalaei et al. 2020). Over 30% increase in IDF ordinate was estimated from HadGEM2-AO model for Han river basin (Lima et al. 2018), and it was observed that precipitation intensity is likely to increase in the future than the current design precipitation intensity over South Korea (Choi et al. 2019). Similar increasing trends in precipitation intensities were observed over selected locations in Brazil (Costa et al. 2020), Turkey (Şen and Kahya 2021), and Malaysia (Shukor et al. 2020).

A few studies had been performed in India as well to capture the changes in IDF. An ensemble from 23 GCMs indicated a 12–53% increase in extreme precipitation of shorter duration for the city of Bangalore (Bengaluru) (Chandra et al. 2015), whereas for Roorkee city in Uttarakhand, the IDF curves estimated from 5 different GCMs showed an increment ranging between 12–96% (Singh et al. 2016). Covariate-based non-stationary analysis of the IDF curves for Hyderabad City exhibited a decrease in return period for extreme precipitation events (Agilan and Umamahesh 2016). About 12% and 87% increase in IDF curves for 2- and 100-year return periods were observed over Chennai city under changing climate (Andimuthu et al. 2019). Except for a few studies concentrated over some individual cities, the existing literature did not explore the spatial and temporal changes of IDF curves in the future across Indian mainland as a whole. This is essential in the context of climate change to understand its spatio-temporal variations and forms the motivation of this study.

The first major issue in this context is the scarcity of sub-daily (hourly) precipitation records, which is essential to generate IDF curves. However, observed hourly precipitation records are not available from most of the data providers, for instance, India Meteorological Department (IMD) provides only up to daily gridded precipitation data across Indian main land (Pai et al. 2014). In such situation, an increasing reliance on the reanalysis data with high temporal and spatial resolution offers an opportunity to overcome this hinderance. A reanalysis is an assimilation of observed records with modern weather forecasting models and data assimilation system, which serves as the best estimate of atmospheric variables. Use of reanalysis data in aforementioned studies is not new. For instance, Kao and Ganguly (2011) studied the IDF changes globally using existing reanalysis datasets with 6-h temporal resolution, and future warming scenarios from Coupled Model Intercomparison Project Phase-3 (CMIP3), which showed a significant impact on IDF curves due to global warming. Courty et al. (2019) used the 5th generation European Centre for Medium-Range Weather Forecasts reanalysis product (ERA5) with temporal resolution in hourly-scale to estimate the IDF curves globally and investigated the scaling relationship of extreme precipitation of different duration. However, global analysis primarily emphasizes the changes at the continental level rather than focusing on the regional level. In addition, none of these studies attempted to quantify the effect of climate change in IDF curves at hourly-scale, which is of utmost importance to understand the climate change effect in a regional scale when short-term extreme precipitation events are notably increasing.

Objective of this study is to assess the spatiotemporal changes in short-duration (hourly) IDF curves under changing climate. Entire Indian mainland is considered as a study area that spans across a wide range of climate regimes, such as deserts on the west, mountainous, plateau in the southern peninsula, world's largest plain in the northern parts, world's highest rainfall receiving zone on the east, etc.. Such a study area is helpful to analyze the spatiotemporal changes in the IDF curves across different climatology (Fig. 1 and Table 1).

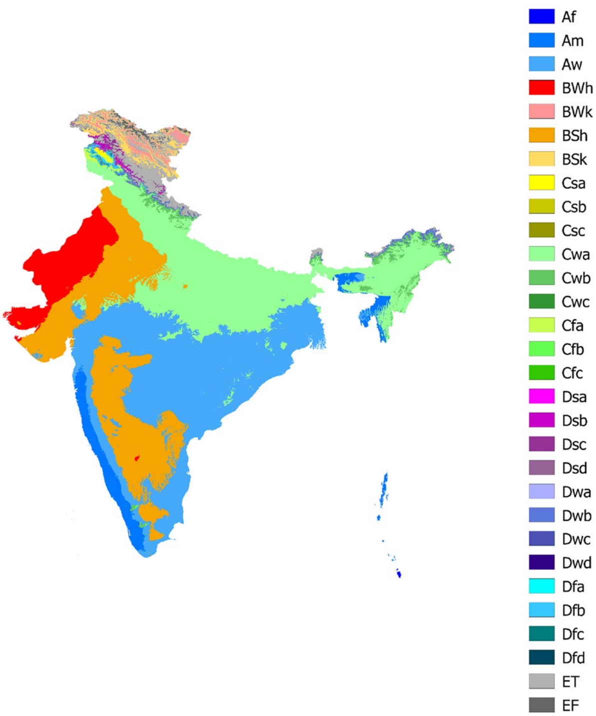

Fig. 1 Köppen-Geiger classifications of India regenerated using the original data from a study by Beck et al. (2018) licensed under a Creative Commons Attribution 4.0 International License, which permits use, sharing, adaptation, distribution and reproduction in any medium or format. The abbreviations are elaborated in Table 1 as per the original study

Table 1 Abbreviation of Köppen-Geiger classifications As per the original paper by Beck et al. (2018) licensed under a Creative Commons Attribution 4.0 International License, which permits use, sharing, adaptation, distribution and reproduction in any medium or format

Abbreviation	Full form	Abbreviation	Full form
Af	Tropical, rainforest	Cfc	Temperate, no dry season, cold summer
Am	Tropical, monsoon	Dsa	Cold, dry summer, hot summer
Aw	Tropical, savannah	Dsb	Cold, dry summer, warm summer
BWh	Arid, desert, hot	Dsc	Cold, dry summer, cold summer
BWk	Arid, desert, cold	Dsd	Cold, dry summer, very cold winter
BSh	Arid, steppe, hot	Dwa	Cold, dry winter, hot summer
BSk	Arid, steppe, cold	Dwb	Cold, dry winter, warm summer
Csa	Temperate, dry summer, hot summer	Dwc	Cold, dry winter, cold summer
Csb	Temperate, dry summer, warm summer	Dwd	Cold, dry winter, very cold winter
Csc	Temperate, dry summer, cold summer	Dfa	Cold, no dry season, hot summer
Cwa	Temperate, dry winter, hot summer	Dfb	Cold, no dry season, warm summer
Cwb	Temperate, dry winter, warm summer	Dfc	Cold, no dry season, cold summer
Cwc	Temperate, dry winter, cold summer	Dfd	Cold, no dry season, very cold winter
Cfa	Temperate, no dry season, hot summer	ET	Polar, tundra
Cfb	Temperate, no dry season, warm summer	EF	Polar, frost

Analysis is carried out for several durations (starting from 1 h) and returns level (starting from 2 years) for analyzing the effects of climate change on IDF curves. Finally, the maps depicting the future changes of hourly precipitation intensity with 2- and 100-year return periods are shown for both the two reanalysis datasets, which may be valuable for updating the design standards, as needed.

2 Data Description

We have used ERA5 reanalysis dataset (Hersbach et al. 2020) and recently released Indian Monsoon Data Assimilation and Analysis (IMDAA) reanalysis dataset (Rani et al. 2021) as reference to bias correct GCM simulated precipitation data for the historical and future period. The ERA5 is a global reanalysis product developed using the Integrated Forecast System (IFS) cycle 41r2 with 4-D-Var data assimilation by European Centre for Medium-Range Weather Forecasts (ECMWF) project. The IMDAA is a regional atmospheric reanalysis over the Indian subcontinent. It is developed by National Centre for Medium Range Weather Forecasting (NCMRWF), India, in collaboration with the Met Office (MO), UK, and the IMD under the National Monsoon Mission (NMM) project of the Ministry of Earth Sciences, Government of India. Observational data from the European Centre for Medium-Range Weather Forecasts (ECMWF) archive and some exclusive observations from the IMD/NCMRWF archives were used to produce the IMDAA reanalysis product (Rani et al. 2021). The IMDAA has performed well in capturing the mean and extreme precipitation events over complex terrain; however, comparison at hourly scale is limited due to the lack of observational data (Rani et al. 2021).

Hourly precipitation data are obtained from both the reanalysis datasets, i.e., ERA5 and IMDAA. The ERA5 is available from 1979 to the present date (https://cds.climate.copernicus.eu/cdsapp#!/dataset/reanalysis-era5-single-levels accessed in August 2021) at a horizontal resolution of 0.25°×0.25° for the atmospheric variables. The IMDAA is available at a horizontal resolution of 0.12°×0.12° for the entire Indian mainland (https://rds.ncmrwf.gov.in/home/ accessed in August 2021). Although both datasets captured the mean rainfall pattern across India well, IMDAA overestimates the daily extreme in northern India and underestimates it in the western ghat region as compared to ERA5 (Singh et al. 2021).

Future simulated precipitation values are obtained from three GCMs, participating in the 6th phase of Coupled Model Intercomparison Project (CMIP6) for three different climate change scenarios, which are combinations of Shared Socioeconomic Pathways (SSPs) and Representative Concentration Pathways (RCPs), namely SSP126, SSP245, SSP585. SSP126 (SSP1+RCP2.6) is the most optimistic scenario which represents sustainable development with a low level of greenhouse gas emission, SSP245 (SSP2+RCP4.5) represents a moderate world with an intermediate level of emission, and SSP585 (SSP5+RCP8.5), which is the most extreme scenario, represents a society with rapid fossil fuel-based development with the highest level of greenhouse gas emission (Riahi et al. 2017; Li et al. 2020).

The model simulated daily precipitation values are downloaded from the World Climate Research Program (WCRP) (https://esgf-node.llnl.gov/projects/cmip6/ accessed in August 2021) for the historical (1979–2014) and future (2015–2100) periods. Outputs from three climate models, i.e., EC-Earth3, CESM2-WACCM and MPI-ESM1-2-HR are considered. A brief description of the climate models is presented in Table 2. Before proceeding

Table 2 Details of the GCMs and climate change scenarios used in this study

Model Name	Source Institution	Default model resolution (lat. × lon.)	Regridded Resolution (lat. × lon.)	Climate change scenarios
EC-Earth3	EC-Earth-Consortium	0.70º × 0.70º	0.25º × 0.25º	SSP126, SSP245, SSP585
CESM2-WACCM	National Center for Atmospheric Research, Climate and Global Dynamics Laboratory, Boulder, USA	0.9424º × 1.25º	0.25º × 0.25º	SSP126, SSP245, SSP585
MPI-ESM1-2-HR	Max Planck Institute for Meteorology, Hamburg, Germany	0.935º × 0.9375º	0.25º × 0.25º	SSP126, SSP245, SSP585

with the analysis, all the datasets are regridded to a common resolution of 0.25°×0.25° to address the resolution mismatch between the reanalysis data and the climate model outputs, using the first-order conservative interpolation scheme ("remapcon" command of the Climate Data Operators software), which is often used in climate studies (Bador et al. 2015; Schoetter et al. 2015; Ring et al. 2018). The period from 1979 to 2014 (36 years) is selected as the historical baseline, considering the available data records.

3 Methodology

Initially the Annual Maximum Series (AMS) of precipitation intensity over moving windows of 1-, 2-, 3-, 6-, 9-, 12- and 24-h duration is extracted from the regridded hourly data for each grid point. The future period is divided into three time periods, i.e., 2015–2039 (immediate future), 2040–2059 (near-future) and 2060–2100 (far-future), and the daily annual maximum series is extracted for each time period and climate scenarios after correcting the model simulated bias. The entire methodological approach is summarized in a flowchart as shown in Fig. 2. Sequentially, these are i) bias correction of GCM simulation, ii) application of AMS and Reliability Ensemble Average (REA) method to obtain the weighted AMS from ensemble of GCM outputs for the historical and future periods, iii) and iv) probabilistic treatment of data through Generalized Extreme Values (GEV) distribution, and v) quantification of spatiotemporal change in IDF curves. The probabilistic treatment of data includes two parts - fitting with GEV distribution to AMS using method of L-moments and scale-invariance model for the scaling relationship between daily and hourly precipitation intensity during the historical period. Using this relationship, future hourly-scale precipitation intensities with various return periods are obtained from daily-scale precipitation intensity. All these the steps are elaborated in the following subsections.

3.1 Bias Correction of GCM Simulated Data

Underestimation or overestimation of model simulated hydrological variables with regard to available observed data is called bias. Despite recent advancements in model simulation, climate models continue to have major biases, owing mostly to a lack of knowledge of physical processes and coarse grid resolution (Addor et al. 2016; Maity et al. 2019). Use of model simulated data without bias correction as input in any model can significantly impact the outcome (Hagemann et al. 2011; Rojas et al. 2011). Hence bias correction of model simulated climate variables is a standard practice before proceeding with further analysis. Bias correction techniques can be broadly categorized as linear, non-linear and distributional quantile mapping (QM) (Kim et al. 2019; Maity et al. 2019; Mishra et al. 2020). Among these, distributional QM technique is widely utilised because of its ease of use and good efficacy in eliminating biases from simulated data (Mearns et al. 2013; Pierce et al. 2015; Shin et al. 2019; Mishra et al. 2020).

In this study, mixed distribution-based QM technique is used for bias correction. This method utilizes a combination of Gamma and Gumbel distribution to correct the bias in mean and extreme precipitation separately (Shin et al. 2019). The Gumbel distribution is applied to bias correct the extreme values (values above 95^{th} percentile), whereas gamma

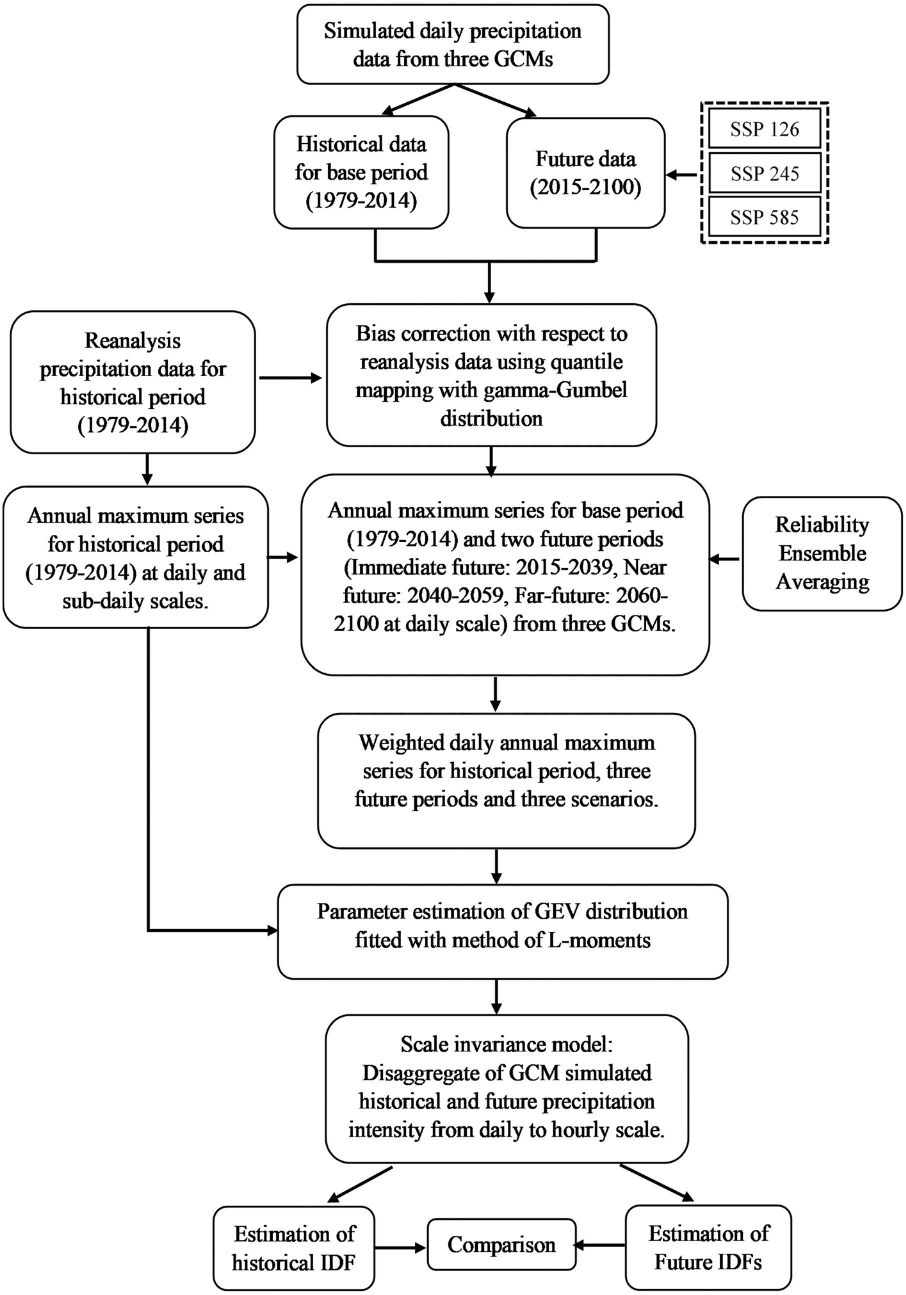

Fig. 2 Methodological flowchart outlining major steps

distribution is applied to the rest, excluding zero values. In QM method, first, the probability distribution of the historical model output from GCM is adjusted in relation to the probability distribution of the observed data by matching the cumulative distribution function.

Subsequently, the future simulations are adjusted based on the transfer function obtained from the first step. In this study, considering the common period of available data from the reanalysis product and historical GCM simulations, we choose 1979–2014 as the base period to bias-correct the future data (2019–2100) separately with respect to ERA5 and IMDAA.

In general, the QM approach for bias correction can be expressed as:

$$x_{bc,GCM} = F_{obs}^{-1}\left(F_{b,GCM}\left(x_{f,GCM}\right)\right) \tag{1}$$

where $x_{bc,GCM}$ and $x_{f,GCM}$represent the bias-corrected and raw future data, respectively. F_{obs}^{-1} is the inverse of CDF for the observed data and $F_{b,GCM}$ is the CDF of the model output for the base period. In this study, initially, the hourly precipitation data are aggregated to obtain the daily precipitation data. Then, the historical model simulated precipitation data is bias-corrected with respect to reanalysis data. Precipitation values above the 95$^{\text{th}}$ percentile are bias-corrected using Gumbel distribution, and the rest are corrected using two-parameter gamma distribution. Finally, the future data is bias-corrected following Eq. (1).

The CDF of Gumbel distribution can be expressed as:

$$F_{gu}(x) = \exp\left[-\exp\left(-\frac{x-\alpha}{\beta}\right)\right] \tag{2}$$

where α and β are the location and scale parameters, respectively.

The CDF of the gamma distribution can be expressed as:

$$F_g(x) = \int_0^x \frac{\beta^\kappa}{\Gamma(\kappa)} x^{\kappa-1} \exp\left(-\frac{x}{\beta}\right) dx;\ x, \beta, \kappa > 0 \tag{3}$$

where β and κ are scale and shape parameters respectively and $\Gamma(*)$ is the gamma function. This process is repeated for each grid covering all the three models and scenarios to bias correct the historical and future precipitation values.

3.2 Reliability Ensemble Averaging

A total of 30 AMS are derived from bias-adjusted daily precipitation values from each of the climate model, one for each scenario (three), coupled with future periods (three), and one for the historical period. The REA method is applied to address the inter-model uncertainty (Chandra et al. 2015). Unlike simple ensemble mean, which gives equal weightage to all the models, the REA method distributes the weights across the models based on two criteria, i.e., model performance and model convergence (Giorgi and Mearns 2002). Model performance criteria assign initial weights to the models based on their ability to simulate present-day climate, while model convergence criteria modify the initial weights until they converge with respect to the future simulation. Giorgi and Mearns (2002) applied this method to address the inter-model uncertainty of temperature and precipitation over 22 regions across the globe considering the A2 and B2 climate change scenarios of the 4$^{\text{th}}$ assessment report of the Intergovernmental Panel on Climate Change (IPCC). However, in the aforementioned study, the weights were assessed based on the mean values only. Some studies used information based on cumulative distribution functions (CDF) instead of mean only (Ghosh and Mujumdar 2009). Later, Chandra et al. (2015) applied REA for total 85 future simulations to obtain the weight-averaged AMS to assess the IDF changes in the future over Bengaluru City. In many studies, the original or modified versions of the REA technique is adopted to address the inter-model uncertainty of future GCM simulations (Kim and Lee 2010; Exbrayat et al. 2018; Tegegne et al. 2019).

We used the modified REA technique on each grid point separately to address the inter-model uncertainty for individual climate change scenarios and timelines obtained from the three climate models after bias correction. The algorithm of the REA method is explained in the following steps:

(i) First, the CDF deviation of the observed daily AMS from the historically simulated series is measured in terms of Root Mean Square Error (RMSE) for 100 equally spaced data points covering the whole range of data and the initial weights are calculated by taking the reciprocal of the RMSE.
(ii) Weights are proportionately assigned to the GCMs, with the sum of the weights equal to 1 across all GCMs.
(iii) Weights obtained in step 2 are multiplied with the CDFs derived from the future values to generate the future weighted mean CDF.

$$F_{wm} = \sum_{i=1}^{n} w_i \times F_{GCM_i} \tag{4}$$

where F_{wm} is the weighted mean CDF of future values, w_i is the weight assigned to the i^{th} GCM and F_{GCM_i} is the CDF of the i^{th} GCM.
(iv) The deviation is calculated for the future period between CDF of individual GCM and weighted mean CDF by calculating the RMSE. The average of the inverse RMSE derived in steps (i) to (iii) are calculated and proportionately assigned as new weights across the GCMs, keeping the sum of weights equal to 1.
(v) Steps (iii) to (iv) are repeated until the weights converge.
(vi) This process is repeated for the three climate change scenarios and three future periods.

Finally, the weighted mean AMS for three future periods are constructed by summing up the weighted AMS corresponding to each climate change scenario.

3.3 Estimation of Generalized Extreme Value (GEV) Distribution Parameters

GEV distribution belongs to the family of extreme value distribution, and it is widely used in hydrological studies to estimate IDF curves from AMS of different duration and return periods (Semmler and Jacob 2004; Kao and Ganguly 2011; Shrestha et al. 2017; Cook et al. 2020; Gaur et al. 2020; Hosseinzadehtalaei et al. 2020). The CDF of GEV distribution is expressed as:

$$F(i) = exp\left[-\left(1+\kappa\left(\frac{i-\alpha}{\beta}\right)\right)^{-\frac{1}{\kappa}}\right] \text{ for } \kappa \neq 0 \tag{5}$$

where α, β and κ are the location, scale and shape parameters, respectively. When κ = 0, GEV distribution represents Gumbel distribution. Studies demonstrate that the estimates from the two-parameter Gumbel distribution show a smaller error than the three-parameter GEV distribution due to the difficulties in assessing the shape parameter owing to a small length of records (Lu and Stedinger 1992; Papalexiou and Koutsoyiannis 2013). However, the use of Gumbel distribution could underestimate the precipitation intensity for long return periods (Koutsoyiannis 2004). Papalexiou and Koutsoyiannis (2013) showed that the value of the shape parameter of GEV distribution could be approximated to 0.114 irrespective of geographic location. To avoid unrealistic estimation of precipitation intensity for different return periods due to incorrect shape parameters, we assumed that AMS follows the GEV distribution with $\kappa = 0.114$ for all the durations. The location parameters (α) and scale parameters (β) are estimated keeping $\kappa = 0.114$ using the method of L-moments, which is less sensitive to sample variability of the extreme values and yields better estimation compared to other methods in case of small sample sets (Hosking 1990). The parameters of GEV distribution are estimated using the following equations given by Hosking (1990):

$$\beta = \frac{l_2 \kappa}{(1 - 2^{-\kappa})\Gamma(1 + \kappa)} \tag{6}$$

$$\alpha = l_1 + \frac{\beta[\Gamma(1 + k) - 1]}{\kappa} \tag{7}$$

wherel_1 and l_2 are the sample L-moment estimate of first-order and second-order, respectively (Hosking 1990) and $\Gamma(.)$ is the gamma function. The values of l_1 and l_2 are computed using Python "lmoments3" library. Kolmogorov–Smirnov (K-S) test is applied to check the goodness-of-fit of GEV distribution (Massey 1951) at a 5% significance level. The K-S test is a nonparametric test that measures the maximum absolute difference between the empirical CDF and the CDF obtained from assumed distribution. If the maximum difference is greater than the critical value, the null hypothesis that the data comes from the assumed distribution is rejected for the desired significance level.

3.4 Scale-Invariance Model for GEV Distribution

One major issue in assessing the future changes of the IDF relationship is the unavailability of hourly precipitation data from the climate models. This shortcoming led to the development of several methods to approximate precipitation statistics from daily-scale to sub-daily scales, such as the K-Nearest-Neighbour (KNN) Weather Generator (WG) algorithm (Peck et al. 2012), discrete multiplicative random cascade model (Molnar and Burlando 2005), Equidistance Quantile Matching Method (Srivastav et al. 2014), Bartlett-Lewis Rectangular Pulse (BLRP) model (Koutsoyiannis and Onof 2001; Ritschel et al. 2017), Scale-invariance model (Gupta and Waymire 1990). Among the methods mentioned above, the scale-invariance model is one of the simplest, yet accurate method and successfully used in numerous studies, even in the recent past (Yu et al. 2004; Blanchet et al. 2016; Ghanmi et al. 2016; Lima et al. 2018; Cannon and Innocenti 2019; Choi et al. 2019; Courty et al. 2019). Scale invariance implies that statistical properties of extreme precipitation for different duration are related to each other by a scale ratio. By definition, $f(t)$ is scale-invariant, if for all positive values of λ, $f(t)$ is proportional to scaled function $f(\lambda t)$ (Yeo et al. 2021). The values of t and λt represent lower and higher temporal resolution, respectively. Mathematically, it can be written as:

$$f(t) = \lambda^{-\theta} f(\lambda t) \tag{8}$$

where *f(t)* and *f(λt)* have same distribution. λ is the scale factor (e.g. if $t=24$ h, $\lambda t=1$ h, then $\lambda=1/24$) and θ is the scaling exponent. Equation (8) can be rewritten in terms of moments as following (Gupta and Waymire 1990):

$$E[f(t)^q] = \lambda^{-\theta(q)} E[f(\lambda t)^q] \tag{9}$$

where q represents the order of moment and $E[f(t)^q]$and $E[f(\lambda t)^q]$ denotes the Non-Central Moments (NCMs) of order q. Log-linearity of NCMs with duration indicates a scaling property of extreme precipitation, and linear relationship between scaling exponent (θ) and order of moments (q) implies simple scaling. (Gupta and Waymire 1990). In the present study, we adopt the scaling method to derive the sub-daily scale precipitation statistics using GEV distribution. The scaled GEV distribution parameters (κ, β, α) and precipitation intensities (*I*) for the *T* year return period can be expressed as following (Yeo et al. 2021):

$$\kappa(\lambda t) = \kappa(t) \tag{10}$$

$$\beta(\lambda t) = \lambda^{\theta} \beta(t) \tag{11}$$

$$\alpha(\lambda t) = \lambda^{\theta} \alpha(t) \tag{12}$$

$$I_T(\lambda t) = \lambda^{\theta} I_T(t) \tag{13}$$

where I_T is the magnitude of precipitation intensity for T year return period, calculated by taking the inverse of the CDF of GEV distribution function which is expressed as following:

$$I_T = \alpha - \frac{\beta}{\kappa}\left(1 - \left[-ln\left(1 - \frac{1}{T}\right)\right]^{-\kappa}\right) \tag{14}$$

The parameter λ^{θ} can be estimated as the ratio of first order NCMs of daily and sub-daily duration and expressed as:

$$\lambda^{\theta} = \frac{\mu_1(\lambda t)}{\mu_1(t)} \tag{15}$$

where $\mu_1(\lambda t)$ and $\mu_1(t)$ are the first order NCMs for sub-daily and daily scale.

3.5 Quantification of Spatiotemporal Change in IDF Curves

In order to quantify the impact of climate change on IDF curves, historical and future IDF curves for three climate change scenarios and three future time periods are compared at each grid point in terms of absolute and percentage change. Plotting these values at each grid point will provide the spatiotemporal changes in IDF (with a specific duration and return period) across Indian mainland. Entire available historical period, i.e., 1979–2014 is considered to determine the historical IDF curves. The GEV distribution is fitted to the AMS of 1-, 2-, 3-, 6-h, 9-h, 12- and 24-h duration using the L-moment method as discussed in Sect. 3.3. The magnitude of precipitation intensity for return period of 2-, 25-, 50- and 100-year is calculated using Eq. (14). For each scenario and future time period, the daily precipitation intensities for the same return periods are determined following the same procedure. The sub-daily estimates are generated as per the simple-scaling relation, mentioned in Sect. 3.4 using Eq. (13).

4 Results and Discussion

4.1 Bias Correction

The bias in the model-simulated precipitation with respect to two reanalysis precipitation datasets (base period of 1979–2014) is assessed on the basis of difference in mean of daily AMS at each grid point. The results are presented in Fig. 3a, b for IMDAA and ERA5, respectively. In both the cases, significant bias in all the three models is noticed during the base period. It is evident from the figures that the EC-Earth3 model overestimates (positive bias) the precipitation magnitudes in the western ghats region and underestimates (negative bias) across the rest of Indian mainland. The CESM2-WACCM model outputs exhibit an opposite characteristic compared to EC-Earth3 model outputs. The MPI-ESM1-2-HR model consistently underestimates the precipitation magnitudes all across the Indian mainland.

Such biases are corrected and the mean of the daily AMS after bias-correction is presented in the third column of Fig. 3a, b for IMDAA and ERA5, respectively. A comparison between the bias before and after bias-correction is also presented in the last two columns of the same figures. Near-zero values of the remaining bias for all the models indicate that the combination of Gamma and Gumbel distribution-based QM technique can successfully correct the bias in extreme precipitation values. Following the similar procedure, the future precipitation values for the period of 2015–2100 are also corrected, separately for each scenario.

4.2 Determination of Model Weights Using REA Method

The inter-model uncertainty is addressed using REA method. First, the daily AMS is extracted from the bias-corrected simulations for the base period and two future periods (near- and far- future), considering each climate change scenarios. Following the method described in methodology, the weights of each GCMs are computed at each grid point considering both the model performance and convergence criteria. The measured model weights are used to construct weighted daily AMS for the historical period, and immediate-future, near-future and far-future periods at each grid point for each climate change scenario. Figures S1 and S2 in the supplementary material shows the spatiotemporal variation of the weights assigned to the GCMs for the three climate change scenarios and two future time periods. For example, higher weights are assigned to the EC-Earth3 model in the western ghats regions of India as compared to other two models in case of SSP585 scenario during the immediate-future and near-future period. Similarly, higher weights are assigned to MPI-ESM1-2-HR model as compared to the CESM2-WACCM model in the western (Gujarat region) and northern plain region during the far-future period. The assigned weights to a particular model also vary spatially and temporally for different combinations of scenarios. For example, weights assigned to the CESM2-WACCM model for the far-future period under SSP585 scenario are visibly higher than that under SSP126 and SSP245. The inter-model and spatiotemporal variation of assigned weights indicate that the simple ensemble mean may not be sufficient to quantify the inter-model uncertainty.

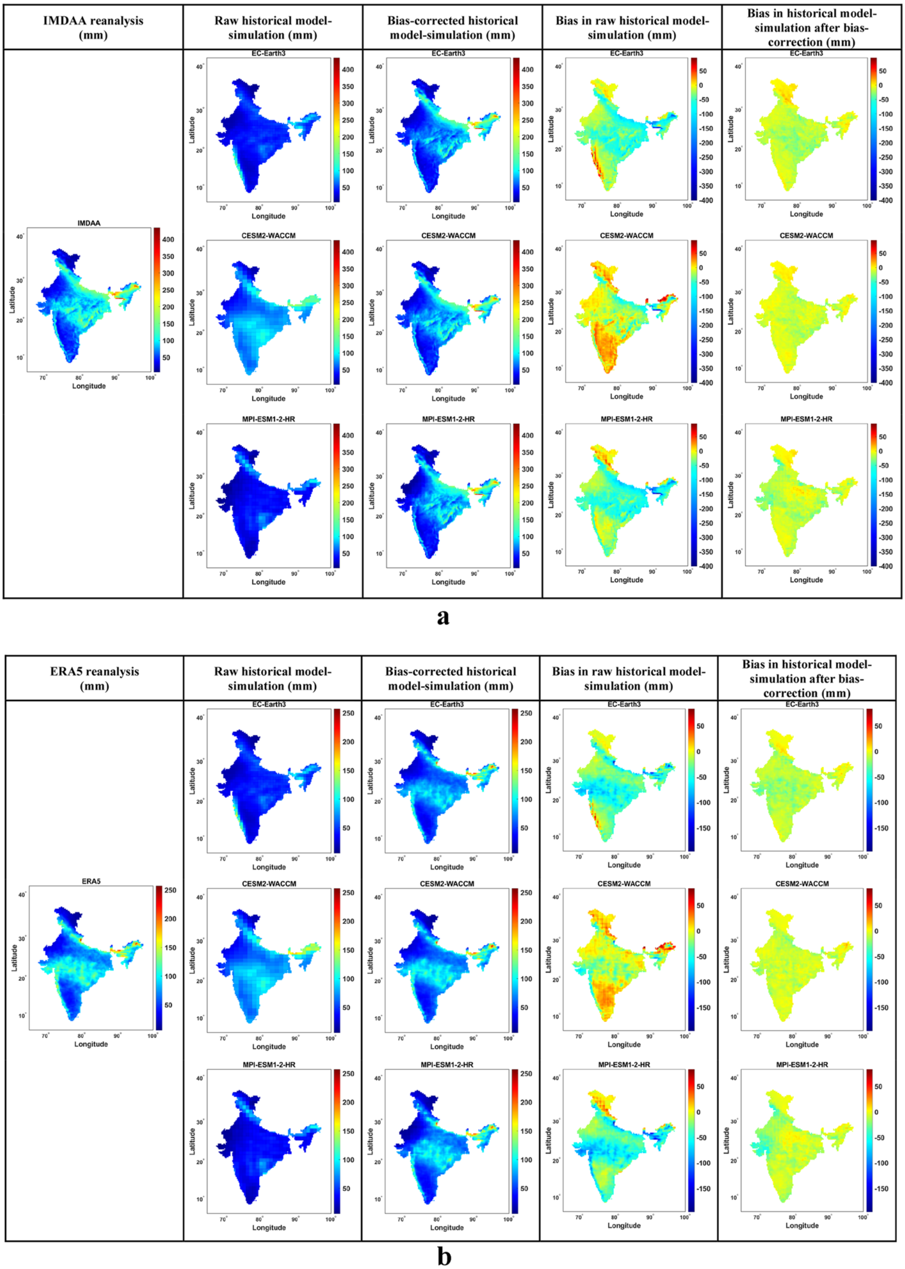

Fig. 3 **a** Bias-correction of GCM simulated precipitation data with respect to IMDAA reanalysis across India evaluated in terms of the mean of daily Annual Maximum Series (AMS) considering 1979–2014 as the base period. **b** Same as Fig. 3a but with respect to the ERA5 reanalysis

Table 3 Percentage of grid points where K-S test does not reject the null-hypothesis that the data comes from GEV distribution at 5% significance level for historical period

Data Source	Duration (hr)						
	1	2	3	6	9	12	24
IMDAA (1979–2014)	98.98	96.84	94.91	90.98	90.46	90.40	92.41
ERA5 (1979–2014)	99.67	95.82	95.36	96.55	93.65	95.60	96.77

Another important observation is that the patterns of assigned weights more or less agree to each other for both the reanalysis datasets.

4.3 Parameter Estimation of GEV Distribution and Goodness of Fit Test

The GEV distribution with a fixed shape parameter ($\kappa = 0.114$) is fitted to the historical (1979–2014) and future (immediate-future, near-future & far-future) AMS for all concerned durations and scenarios using the method of L-moments, and the goodness-of-fit of the distribution is assessed with K-S test at 5% significance level, as described in methodology section.

Tables 3 and 4 present the percentage of grids points where K-S test does not reject the null-hypothesis that the data comes from the GEV distribution at 5% significance level at 5% significance level for historical and future periods, respectively. The result shows that percentage of grids range from 90 to 99% where the AMS can be assumed to follow GEV

Table 4 Percentage of grid points where K-S test does not reject the null-hypothesis that the data comes from GEV distribution at 5% significance level for future periods at daily scale

Reference Data Source	Data Period	Scenarios		
		SSP126	SSP245	SSP585
IMDAA	Immediate-future (2015–2039)	99.98	99.98	99.98
	Near-future (2040–2059)	99.87	99.98	100.00
	Far-future (2060–2100)	99.96	99.93	99.93
ERA5	Immediate-future (2015–2039)	99.96	99.96	99.93
	Near-future (2040–2059)	99.70	99.93	99.98
	Far-future (2060–2100)	99.91	999.93	99.91

Table 5 Percentage of grid points showing linearity between log-transformed NCMs and durations for five orders of moments with respect to R^2 values

Data Source	Range of R^2	NCM 1	NCM 2	NCM 3	NCM 4	NCM 5
IMDAA (1979–2014)	≥ 0.85	100	100	99.80	99.07	98.09
ERA5 (1979–2014)	≥ 0.85	99.67	99.41	96.44	90.98	85.06

distribution at 5% significance level for both the reanalysis products as well as weighted future data. Hence, it is reasonable to accept that the GEV distribution with shape parameter κ = 0.114 could be used for IDF derivation for the entire Indian mainland.

4.4 Changing Pattern in IDF Relationship

4.4.1 Simple-scaling and Generation of IDF Curves

To estimate the change in the IDF in future, simple scaling behavior of extreme precipitation is examined for the historical period (1979–2014) following the method explained in the methodology section. The existence of scaling between 1-h and 24-h precipitation extremes are examined by measuring the coefficient of determination (R^2) between log-transformed values of NCMs and durations for five orders of moments. Table 5 shows that more than 90 percent of the grids for the five NCMs show the value of R^2 greater than 0.85 for both the reanalysis datasets, which supports the existence of a scaling relation between daily and hourly extreme precipitation. Similarly, the simple scaling assumption is tested by checking the linearity between scaling exponents and order of moments; it also holds true for 99% grids, showing R^2 value more than 0.9. Figure 4 shows the spatial variation of R^2 value for the simple scaling assumption. After validation of simple-scaling property, parameter λ^{β} is calculated for sub-daily scales using Eq. (15), as explained in methodology section.

To examine the changes, first, using the scale-invariance relation derived from reanalysis datasets, precipitation intensities at sub-daily scales are estimated from daily scales for historical and future periods considering 2-, 25-, 50-, and 100-year return periods. For the historical and future periods, precipitation intensities at daily scale are generated using Eq. (14) for the concerned return periods. Subsequently, the sub-daily scale precipitation intensities are obtained by multiplying the daily scale intensities with parameter λ^{θ} as shown in Eq. (13). This process is repeated for each grid points to obtain the spatial variation of

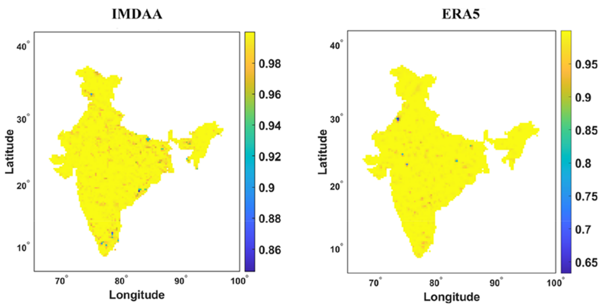

Fig. 4 Spatial distribution of linear association between scaling exponents (θ) and order of moments (q) over India, indicating existence of simple scaling

IDF. Lastly, two sets of IDF datasets are obtained for both historical and future periods from the CMIP6 simulations based on the reference reanalysis data used for bias-correction (i.e. ERA5 and IMDAA), and the changes in future IDFs relative to the historical period are presented in terms of absolute and percentage change in the following section.

4.4.2 Future IDF Curves and Comparison with the Historical Period

The variations in the 1-h duration precipitation intensity agree with the SSPs and the time periods considered. For SSP126, the most conservative of the three scenarios, the average rise in hourly precipitation intensity considering 100-year return period is 13–14% over 45–52% area in the immediate-future, 16–17% over 54–59% area in the near-future, and 15–16% over 62–68% are in the far-future based on both bias-corrected datasets. The decline in average increase in the far-future for SSP126 agrees with the net-zero CO_2 emission projection in the far-future. For SSP245 and SSP585, the spatial pattern of change in the immediate-future is similar to SSP126 because the projected emission scenario in the immediate-future is same as SSP126. But for near-future and far-future the spatio-temporal change is different for SSP245 and SSP585 due to the difference in CO_2 projection scenario. In the near future, 53–59% of the region shows an average rise of 19–20% for the intermediate scenario SSP 245, while in the far future, it is approximately 21–22%, encompassing 76–83% of the country. However, the average increase in the far-future for the most extreme scenario, SSP585 is around 44–48%, nearly double that of SSP245, and covers almost the whole Indian mainland. Higher increase (≈100–120%) in 1-h precipitation intensity with 100-year return period is observed in the central part of mainland India starting from Gujarat coast followed by parts of northern India near mountainous regions of Uttarakhand, some parts of eastern India and north-east

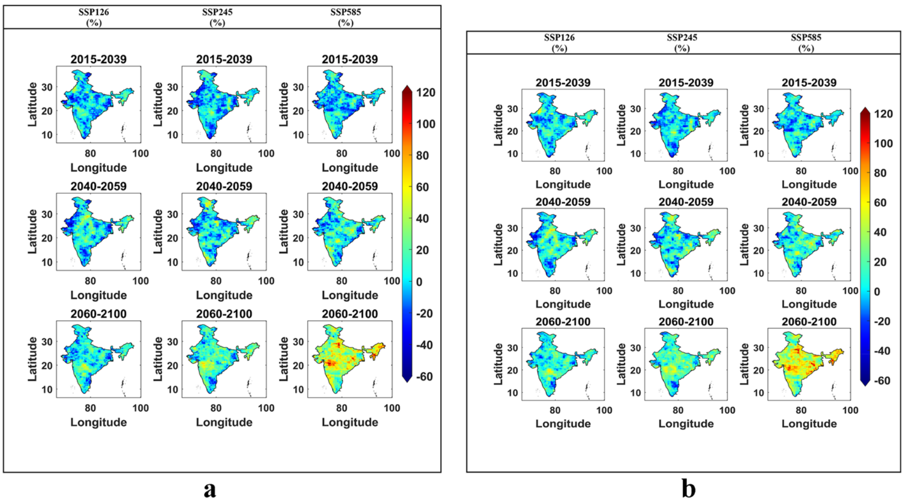

Fig. 5 **a** Percentage change between future (2015–2039, 2040–2059, 2060–2100) and historical (1979–2014) precipitation intensity of 1-h duration for 100-year return period considering three climate change scenarios (bias corrected with reference to IMDAA). **b** Same as Fig. 5a but bias corrected with reference to ERA5

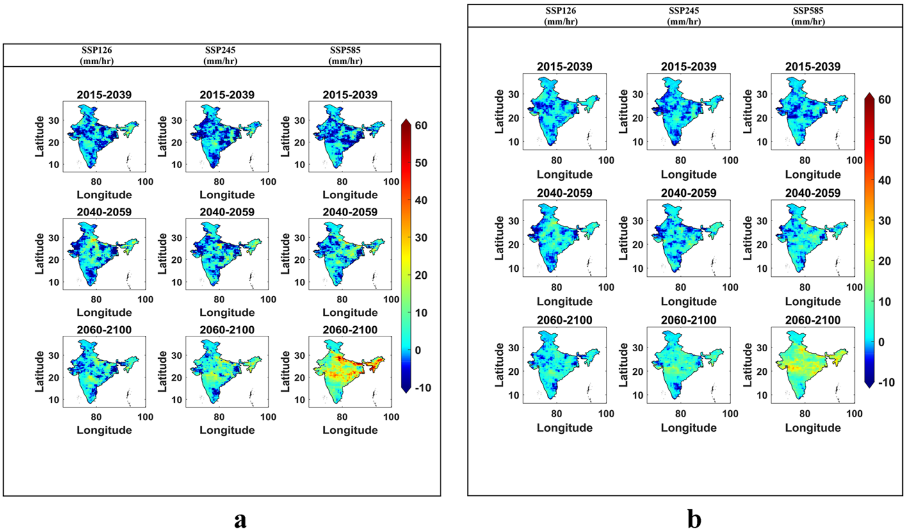

Fig. 6 **a** Absolute change between future (2015–2039, 2040–2059, 2060–2100) and historical (1979–2014) precipitation intensity of 1-h duration for 100-year return period considering three climate change scenarios (bias corrected with reference to IMDAA). **b** Same as Fig. 6a but bias corrected with reference to ERA5

India as shown in Fig. 5a, b (Fig. 6a, b) in terms of percentage change (absolute change in mm/hr). A significant increase is also observed over the arid regions of India which generally receives very less rainfall. The average increase in precipitation intensity for 100-year return period is summarized in Table 6.

Changes in precipitation intensity patterns over the Indian subcontinent for even shorter return periods such as 2-years are consistent with those seen in precipitation with a 100-year return period. The zones with highest increase (≈ 90–120%) are scattered across the central part of India starting from Gujarat and part of Rajasthan followed by Terai regions in the north as shown in Fig. 7a, b (Fig. 8a, b) in terms of percentage change (absolute change). For SSP126 scenario the average increase in precipitation intensity in the immediate-future lies between 8–8.75% covering 64–71% area, which increases in near-future to 12–13% covering almost 74–80% area but decreases in far-future to 11–12% covering almost 85–92% of Indian mainland. However, for SSP245 and SSP585 it continuously increases from immediate-future to far-future. The rise in precipitation intensity is similar to SSP 126 in the immediate-future for SSP245 and SSP585. However, in the near-future for SSP245 it increases to 12.5–13.6% over 82–87% area which further increases to 17–19% covering almost entire mainland in the far-future. Although the increment for SSP585 is similar to SSP245 in the near-future, it nearly doubles in the far-future when compared to SSP245. The average increase in precipitation intensity for 100-year return period is summarized in Table 7.

From the results it is observed that overall, the central part of India starting from Gujarat and Rajasthan (Am, Aw, BWh & BSh; Elaborated in Table 1) will be the worst affected followed by the mountainous regions of north India (Cwa, Cwb, Cwc, ET) as well as parts of northeast India (Cwa & Af) due to increase in precipitation intensity of different return periods. Maximum increase for the worse climate change scenario is evident. Even for the moderate scenario (SSP245), the increase is alarming that prompts us to reconsider the

Table 6 Average percentage increase in 1-h duration, 100-year return period precipitation intensity and corresponding percentage of grid-points for three future periods and three climate change scenarios with respect to historical period

Reference Data for Bias Correction	Climate change scenario	Immediate future (2015–2039)		Near-future (2040–2059)		Far-future (2060–2100)	
		Percentage of grid-points	Average increase	Percentage of grid-points	Average increase	Percentage of grid-points	Average increase
IMDAA	SSP126	45.54	13.81	53.81	16.80	62.03	15.30
	SSP245	42.83	13.25	52.80	19.10	76.01	21.14
	SSP585	42.87	13.28	61.31	18.27	97.29	44.58
ERA5	SSP126	51.86	14.31	58.99	17.73	68.47	16.36
	SSP245	48.20	13.32	59.45	19.59	82.90	21.94
	SSP585	50.30	13.17	67.73	19.00	98.40	48.04

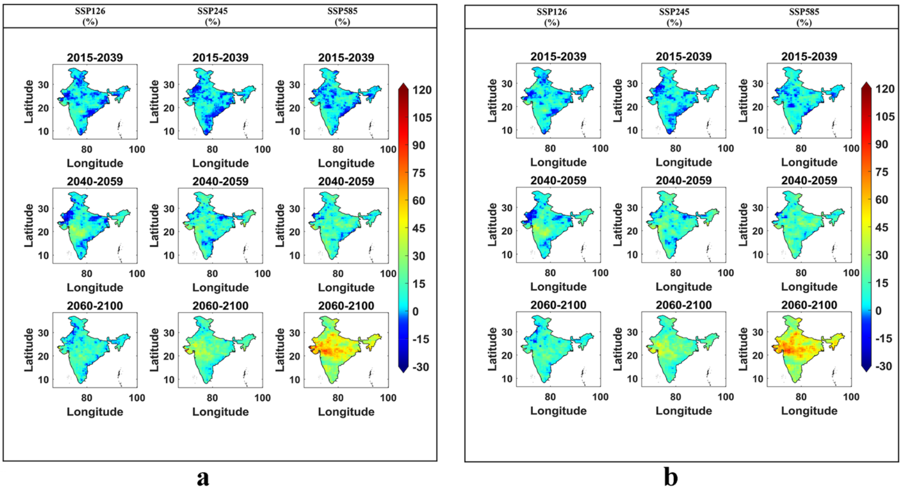

Fig. 7 **a** Percentage change between future (2015–2039, 2040–2059, 2060–2100) and historical (1979–2014) precipitation intensity of 1-h duration for 2-year return period considering three climate change scenarios (bias corrected with reference to IMDAA). **b** Same as Fig. 7a but bias corrected with reference to ERA5

design criteria of different water infrastructure. A similar pattern of spatio-temporal change is observed across the Indian mainland in terms of percentage from both datasets that are bias corrected independently with regard to each reanalysis dataset, which strengthens the conclusion even further.

Similar patterns are noticed for other return periods as well and maps for other return periods can also be prepared in the same manner. However, entire data set is prepared and

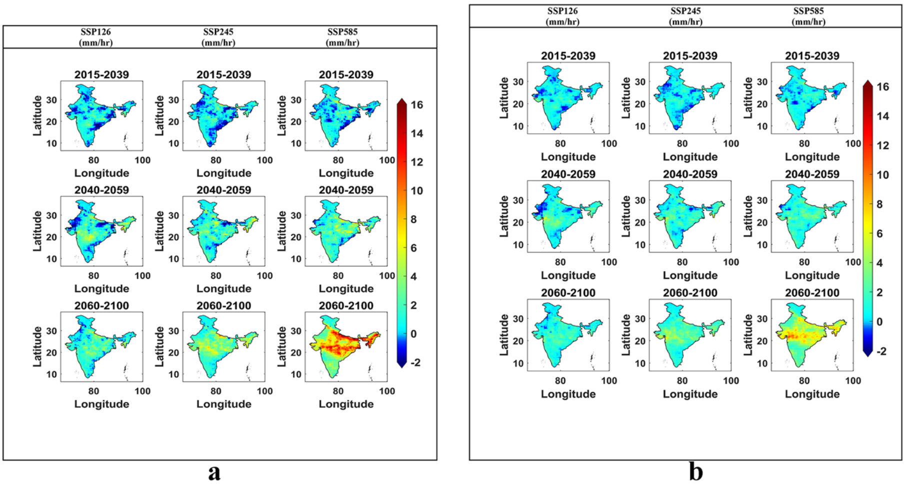

Fig. 8 **a** Absolute change between future (2015–2039, 2040–2059, 2060–2100) and historical (1979–2014) precipitation intensity of 1-h duration for 2-year return period considering three climate change scenarios (bias corrected with reference to IMDAA). **b** Same as Fig. 8a but bias corrected with reference to ERA5

Table 7 Average percentage increase in 1-h duration, 2-year return period precipitation intensity and corresponding percentage of grid-points for three future periods and three climate change scenarios with respect to historical period

Reference Data for Bias Correction	Climate change scenario	Immediate future (2015–2039)		Near-future (2040–2059)		Far-future (2060–2100)	
		Percentage of grid-points	Average increase	Percentage of grid-points	Average increase	Percentage of grid-points	Average increase
IMDAA	SSP126	64.65	8.07	74.43	12.20	85.76	11.22
	SSP245	60.90	7.43	82.51	12.51	97.40	17.96
	SSP585	66.82	8.06	89.97	13.46	99.96	41.28
ERA5	SSP126	71.33	8.75	80.71	12.97	92.33	12.10
	SSP245	68.51	7.85	87.69	13.61	99.05	19.53
	SSP585	76.33	8.40	94.76	14.41	100.00	43.50

kept in an open-source data repository (https://data.mendeley.com/datasets/gg3vy49jzg/draft?a=50c8f564-183a-49d3-8536-598ef40b3a9b).

Next, we have selected four metro cities in India, namely Kolkata, Chennai, Mumbai and New Delhi, to discuss the temporal change IDF under the changing climate. The increase in the IDF curves as observed from the figures suggest that the most populated urban areas will get significantly affected due to climate change. The changes in the far-future for the worst-case scenario considering 2- and 100-year return period for the four metro cities are presented in Fig. 9. The results show that all the cities will experience a significant increase in precipitation intensity in the future. However, the findings considering ERA5 are more reliable than the IMDAA due to its inherent bias in capturing extreme precipitation as discussed earlier. Based on the above observation, IDF curves for the four cities are constructed considering ERA5 as reference data. For brevity, IDF curves for only Kolkata and Mumbai are plotted in the Fig. 10a, b respectively. The IDFs for the city of Chennai and New Delhi are presented in Figs. S3 and S4 of the supplementary material.

The overall evaluation of the findings suggests that the hourly precipitation intensity will rise significantly in the future for both short and long return periods, and analysis with regard to IMDAA and ERA5 supports this conclusion. The comparison indicates a very alarming situation for the central India encompassing parts of Gujarat, Madhya Pradesh and Maharashtra. Ministry of Earth Sciences (MoES), Government of India reported that Over central India, the frequency of daily precipitation extremes increased by 75% between 1950–2015 (Krishnan et al. 2020). Frequent floods in these states due to heavy rainfall in recent decades indicates that the scenario is already changing (https://www.hindustantimes.com/india-news/why-is-it-flooding-in-central-india/story-KpsDiw5nbu5OaAYdcckaLL.html accessed in August 2022). The arid regions of India

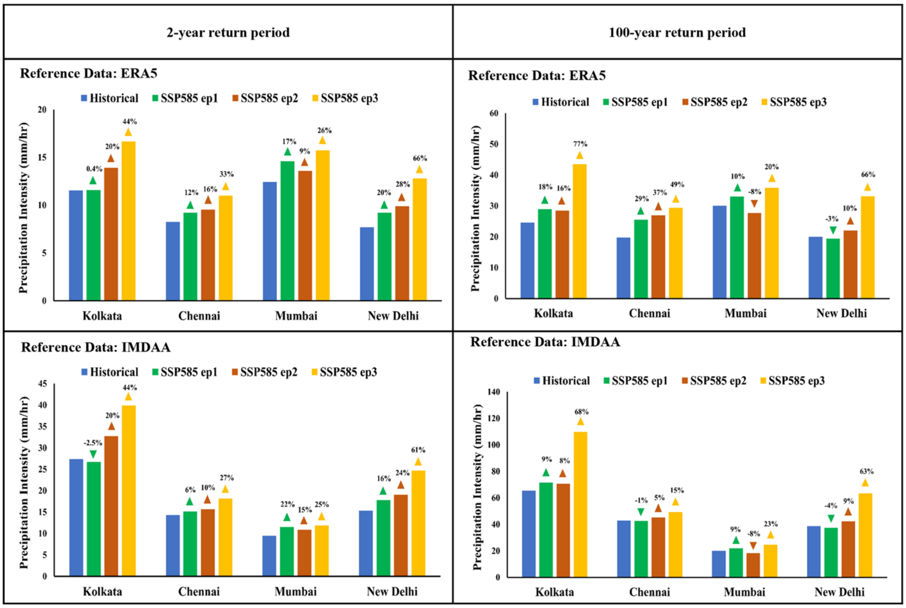

Fig. 9 Precipitation intensity (mm/hr) and the respective percentage change at immediate-future (ep1:2015–2039), near-future (ep2:2040–2059) and far-future (ep3:2060–2100) considering SSP585 scenario with reference to historical data (1979–2014) (Bias corrected with reference to ERA5 and IMDAA reanalysis data). Results obtained from ERA5 are more reliable (for discussion refer the text)

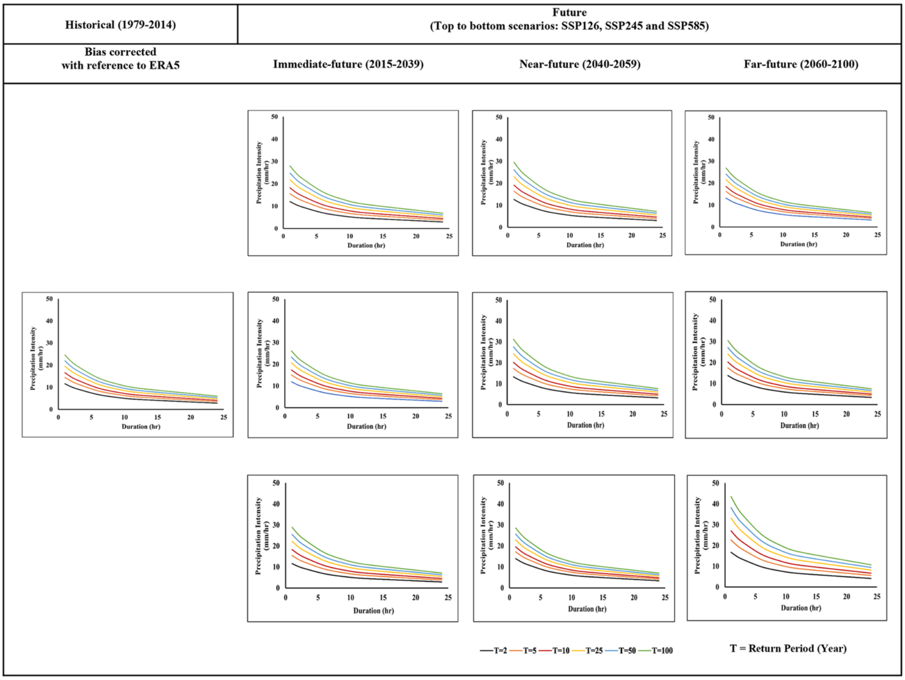

a

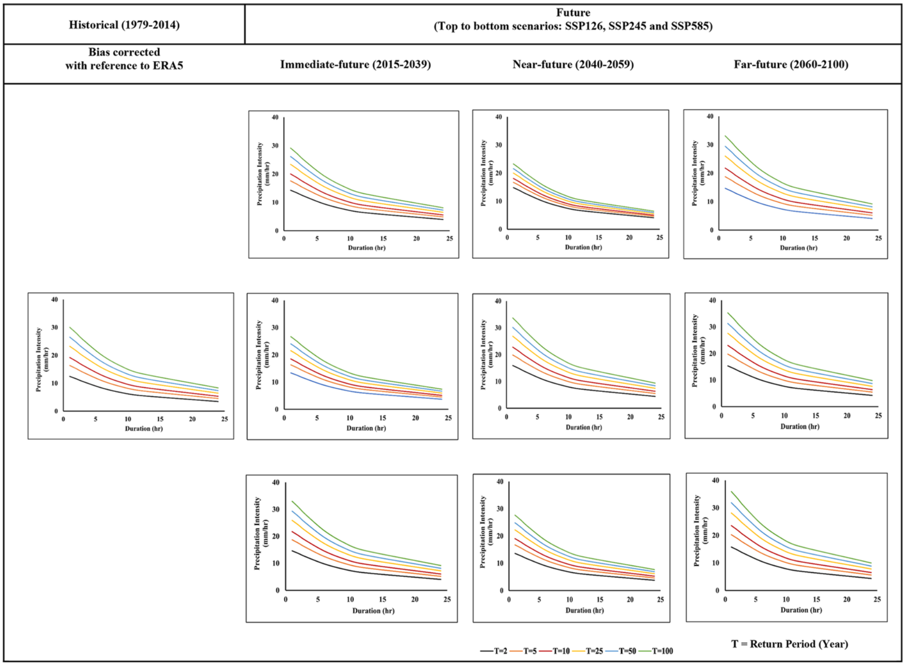

b

Fig. 10 **a** IDF curves for immediate-future (2015–2039), near-future (2040–2059) and far-future (2060–2100) considering three climate change scenarios for City of Kolkata. **b** Same as Fig. 10a but for City of Mumbai in Rajasthan which generally receives very less rainfall annually, is seeing an increase in heavy precipitation and projected to witness a significantly heavy precipitation in the future. The mountainous and Terai regions which already have a fragile ecosystem due to sensitive geology of Himalaya (Poonam et al. 2017) will also witness an increase in extreme precipitation in the future. In 2021, Uttarakhand faced series of flash floods due to glacial lake bursts caused by extreme precipitation of short duration (https://www.ndtv.com/india-news/cloudburst-in-uttarakhands-devprayag-shops-houses-damaged-report-2439704, accessed in May 2021). Devastating floods are witnessed in Bihar and Uttar Pradesh due to high-intensity precipitation in the upstream of Himalayan rivers, resulting in the rise of water levels downstream (https://timesofindia.indiatimes.com/city/patna/nepal-rivers-in-spate-may-flood-swathes-of-bihar-up/articleshow/77098534.cms accessed in May 2021). Further increase in the hourly-precipitation intensity of short return period, as indicated in this study, will make such disasters more frequent. Apart from that, a substantial increase in hourly precipitation intensity for both short and long return period in the highly populated western and central part of India indicates chances of disastrous flash floods in the future which will severely affect the livelihood and economy of the regions.

Precipitation in the mountainous region is dominated by orographic precipitation, and the possible cause behind the significant increase in hourly precipitation intensity can be attributed to the precipitation shift from snow to rain due to climate change in the Himalayan region (Pavelsky et al. 2012). However, this study does not explore the contribution of global and regional effects of climate change separately.

5 Conclusions

How does climate change alter the relationship between intensity, duration and frequency (IDF) of precipitation? This study attempts to explore this question. Spatiotemporal variation of IDF relationships using two reanalysis products from past and model-simulated future precipitation from three CMIP6 models, namely EC-Earth3, CESM2-WACCM & MPI-ESM1-2-HR. Three climate change scenarios, as designated by SSP126, SSP245 and SSP585, are used in case of future precipitation and the inter-model uncertainty is addressed using the REA technique. The changes in precipitation intensity for various return periods (2 to 100 years) are evaluated for immediate-future (2015–2039), near-future (2040–2059) and far-future (2060–2100) periods with respect to the historical period (1979–2014), separately considering CMIP6 dataset bias-corrected separately with respect to two reanalysis datasets.

The comparison with reference to both the reanalysis data shows an average increase of 17% to 21% in precipitation intensity covering around 70–90% of the area under SSP245, whereas for SSP585 the increment is in the range of 40–48%, covering almost entire India. The increase in the precipitation intensity is more in the Central part of India starting from coast of Gujarat, the mountainous regions of Himachal Pradesh and Uttarakhand along with the Terai region and Northeast India under the SSP245 and SSP585 scenario. The great plains of north, southern peninsula and the desert region will also witness a moderate increase in precipitation intensity. On the contrary, SSP126, which assumes sustainable development in the future, shows a minimal increase compared to the other two scenarios. These changes indicate that if the trend of rapid development and uncontrolled use of fossil fuels continues, India will witness a significant increase in hourly precipitation intensity in the future. The ecologically sensitive mountainous regions of India will experience frequent floods than the rest of India as a consequences of climate change. The most populated metro cities will also suffer significantly due to increase in extreme precipitation intensity in the coming future. Entire information on future IDF with respect to latitude, longitude, near- or far-future, scenario of climate change are provided in an open repository (https://data.mendeley.com/datasets/gg3vy49jzg/draft?a=50c8f564-183a-49d3-8536-598ef40b3a9b).

To minimize the impact of increasing extreme precipitation due to climate change, a sustainable development approach should be of utmost priority for future infrastructure development activities. The approaches to incorporate climate change impact in the design of infrastructure may vary significantly from place to place depending on the importance of the place and the cost involved. The most practical approach for mitigating the consequences of climate change is to design and build structures with sufficient flow capacity to handle future flow conditions rather than present flow conditions. However, this strategy comes with lots of uncertainty arising from the data quality, resolution and modelling assumptions which may increase the cost of project rendering it economically unviable. Watt et al. (2003) suggested that in absence of better estimates of precipitation intensity the design storm adopted for design should be 15% larger than the present estimate. However, retrofitting of existing infrastructures to accommodate the increased flow requires more detailed planning because most of the infrastructures are underground thus having constraints related to availability of space to expand and associated costs. Furthermore, non-stationary approach for planning and designing of hydraulic infrastructures should be adopted because stationary assumptions may not provide adequate safety from floods in the context of climate change. However, it should be noted that these conclusions are based on the reanalysis data used, which may be an excellent alternative to compensate for the lack of hourly observational data, but may have a significant difference with respect to the actual scenario. Hence, the interpretation should be more focused on the spatiotemporal pattern of the change rather than the absolute values. Consideration of monsoon and non-monsoon precipitation separately may be a potential further scope of study.

Supplementary Information The online version contains supplementary material available at https://doi.org/10.1007/s11269-022-03313-y.

Acknowledgements We gratefully acknowledge NCMRWF, Ministry of Earth Sciences, Government of India, for IMDAA reanalysis (Rani et al. 2021). IMDAA reanalysis was produced under the collaboration between UK Met Office, NCMRWF, and IMD with financial support from the Ministry of Earth Sciences, under the National Monsoon Mission programme. We are also grateful to ECMWF for making available ERA5 reanalysis datasets (Hersbach et al. 2020). The results contain modified Copernicus Climate Change Service information 2020.

Author Contribution Conceptualization: RM; Methodology: SSM, RM; Formal analysis and investigation: SSM, RM; Writing - original draft preparation: SSM; Writing - review and editing: RM; Funding acquisition: RM; Resources: RM; Supervision: RM.

Funding This work is partially supported by the Ministry of Earth Science, Government of India through a sponsored project.

Availability of Data and Material Hourly precipitation data are obtained from both the reanalysis datasets, i.e., ERA5 (https://cds.climate.copernicus.eu/cdsapp#!/dataset/reanalysis-era5-single-levels accessed in August 2021) and IMDAA (https://rds.ncmrwf.gov.in/home/ accessed in August 2021). The model simulated daily precipitation values are downloaded from the World Climate Research Program (WCRP) (https://esgf-node.llnl.gov/projects/cmip6/ accessed in August 2021).

Code Availability The codes required for the analysis are written in MATLAB R2018a (version 9.4). The codes may be available on request from the authors.

Declarations

Ethics Approval This paper has not been published or is being considered for publication elsewhere.

Consent to Participate The authors declare that they are aware and consent to their participation in this paper.

Consent for Publish The authors declare that they consent to the publication of this paper.

Conflicts of Interest The authors have no relevant financial or non-financial interests to disclose.

References

Addor N, Rohrer M, Furrer R, Seibert J (2016) Propagation of biases in climate models from the synoptic to the regional scale: Implications for bias adjustment. J Geophys Res Atmos 121(5):2075–2089. https://doi.org/10.1002/2015JD024040

Agilan V, Umamahesh NV (2016) Is the covariate based non-stationary rainfall IDF curve capable of encompassing future rainfall changes? J Hydrol 541:1441–1455. https://doi.org/10.1016/j.jhydrol.2016.08.052

Andimuthu R, Kandasamy P, Mudgal BV, Jeganathan A, Balu A, Sankar G (2019) Performance of urban storm drainage network under changing climate scenarios: Flood mitigation in Indian coastal city. Sci Rep 9(1):1–10. https://doi.org/10.1038/s41598-019-43859-3

Arnbjerg-Nielsen K (2012) Quantification of climate change effects on extreme precipitation used for high resolution hydrologic design. Urban Water J 9(2):57–65. https://doi.org/10.1080/1573062X.2011.630091

Asadieh B, Krakauer NY (2015) Global trends in extreme precipitation: Climate models versus observations. Hydrol Earth Syst Sci 19(2):877–891. https://doi.org/10.5194/hess-19-877-2015

Bador M, Naveau P, Gilleland E, Castellà M, Arivelo T (2015) Spatial clustering of summer temperature maxima from the CNRM-CM5 climate model ensembles & E-OBS over Europe. Weather Clim Extremes 9:17–24. https://doi.org/10.1016/j.wace.2015.05.003

Beck HE, Zimmermann NE, McVicar TR, Vergopolan N, Berg A, Wood EF (2018) Present and future Köppen-Geiger climate classification maps at 1-km resolution. Sci Data 5(1):180214. https://doi.org/10.1038/sdata.2018.214

Bertini C, Buonora L, Ridolfi E, Russo F, Napolitano F (2020) On the use of satellite rainfall data to design a dam in an ungauged site. Water (switzerland) 12(11):1–20. https://doi.org/10.3390/w12113028

Bhatkoti R, Moglen GE, Murray-Tuite PM, Triantis KP (2016) Changes to bridge flood risk under climate change. J Hydrol Eng 21(12):04016045. https://doi.org/10.1061/(asce)he.1943-5584.0001448

Blanchet J, Ceresetti D, Molinié G, Creutin JD (2016) A regional GEV scale-invariant framework for Intensity–Duration–Frequency analysis. J Hydrol 540:82–95. https://doi.org/10.1016/j.jhydrol.2016.06.007

Cannon AJ, Innocenti S (2019) Projected intensification of sub-daily and daily rainfall extremes in convection-permitting climate model simulations over North America: Implications for future intensity-duration-frequency curves. Nat Hazard 19(2):421–440. https://doi.org/10.5194/nhess-19-421-2019

Chandra R, Saha U, Mujumdar PP (2015) Model and parameter uncertainty in IDF relationships under climate change. Adv Water Resour 79:127–139. https://doi.org/10.1016/j.advwatres.2015.02.011

Choi J, Lee O, Jang J, Jang S, Kim S (2019) Future intensity–depth–frequency curves estimation in Korea under representative concentration pathway scenarios of Fifth assessment report using scale-invariance method. Int J Climatol 39(2):887–900. https://doi.org/10.1002/joc.5850

Cook LM, McGinnis S, Samaras C (2020) The effect of modeling choices on updating intensity-duration-frequency curves and stormwater infrastructure designs for climate change. Clim Change 159(2):289–308. https://doi.org/10.1007/s10584-019-02649-6

Courty LG, Wilby RL, Hillier JK, Slater LJ (2019) Intensity-duration-frequency curves at the global scale. Environ Res Lett 14(8). https://doi.org/10.1088/1748-9326/ab370a

de Souza Costa CEA, Blanco CJC, de Oliveira-Júnior JF (2020) Idf curves for future climate scenarios in a locality of the Tapajós Basin, Amazon, Brazil. J Water Clim Change 11(3):760–770. https://doi.org/10.2166/wcc.2019.202

Exbrayat JF, Bloom AA, Falloon P, Ito A, Luke Smallman T, Williams M (2018) Reliability ensemble averaging of 21st century projections of terrestrial net primary productivity reduces global and regional uncertainties. Earth Syst Dyn 9(1):153–165. https://doi.org/10.5194/esd-9-153-2018

Fowler HJ, Ali H, Allan RP, Ban N, Barbero R, Berg P, Blenkinsop S, Cabi NS, Chan S, Dale M, Dunn RJH, Ekström M, Evans JP, Fosser G, Golding B, Guerreiro SB, Hegerl GC, Kahraman A, Kendon EJ, Whitford A (2021) Towards advancing scientific knowledge of climate change impacts on short-duration rainfall extremes. Philos Trans Royal Soc a: Math Phys Eng Sci 379(2195):20190542. https://doi.org/10.1098/rsta.2019.0542

Gaur A, Schardong A, Simonovic SP (2020) Gridded extreme precipitation intensity–duration–frequency estimates for the Canadian landmass. J Hydrol Eng 25(6):05020006. https://doi.org/10.1061/(asce)he.1943-5584.0001924

Ghanmi H, Bargaoui Z, Mallet C (2016) Estimation of intensity-duration-frequency relationships according to the property of scale invariance and regionalization analysis in a Mediterranean coastal area. J Hydrol 541:38–49. https://doi.org/10.1016/j.jhydrol.2016.07.002

Ghosh S, Mujumdar PP (2009) Climate change impact assessment: Uncertainty modeling with imprecise probability. J Geophys Res Atmos 114(18). https://doi.org/10.1029/2008JD011648

Giorgi F, Mearns LO (2002) calculation of average, uncertainty range and reliability of regional climate changes from AOGCM simulations via the "reliability ensemble averaging" (REA) method. J Clim 16(5):883–884. https://doi.org/10.1175/1520-0442(2003)016%3c0883:COCOAU%3e2.0.CO;2

Gupta VK, Waymire E (1990) Multiscaling properties of spatial rainfall and river flow distributions. J Geophys Res 95(D3):1999–2009. https://doi.org/10.1029/JD095iD03p01999

Hagemann S, Chen C, Haerter JO, Heinke J, Gerten D, Piani C (2011) Impact of a statistical bias correction on the projected hydrological changes obtained from three GCMs and two hydrology models. J Hydrometeorol 12(4):556–578. https://doi.org/10.1175/2011JHM1336.1

Hersbach H, Bell B, Berrisford P, Hirahara S, Horányi A, Muñoz-Sabater J, Nicolas J, Peubey C, Radu R, Schepers D, Simmons A, Soci C, Abdalla S, Abellan X, Balsamo G, Bechtold P, Biavati G, Bidlot J, Bonavita M, Thépaut JN (2020) The ERA5 global reanalysis. Q J R Meteorol Soc 146(730):1999–2049. https://doi.org/10.1002/qj.3803

Hosking JRM (1990) L-moments: Analysis and estimation of distributions using linear combinations of order statistics. J Roy Stat Soc: Ser B (methodol) 52(1):105–124. https://doi.org/10.1111/j.2517-6161.1990.tb01775.x

Hosseinzadehtalaei P, Tabari H, Willems P (2020) Climate change impact on short-duration extreme precipitation and intensity–duration–frequency curves over Europe. J Hydrol 590(March):125249. https://doi.org/10.1016/j.jhydrol.2020.125249

Kang MS, Koo JH, Chun JA, Her YG, Park SW, Yoo K (2009) Design of drainage culverts considering critical storm duration. Biosys Eng 104(3):425–434. https://doi.org/10.1016/j.biosystemseng.2009.07.004

Kao SC, Ganguly AR (2011) Intensity, duration, and frequency of precipitation extremes under 21st-century warming scenarios. J Geophys Res Atmos 116(16):1–14. https://doi.org/10.1029/2010JD015529

Keller S, Atzl A (2014) Mapping natural hazard impacts on road infrastructure—the extreme precipitation in Baden-Württemberg, Germany, June 2013. Int J Disaster Risk Sci 5(3):227–241. https://doi.org/10.1007/s13753-014-0026-1

Kim DI, Kwon HH, Han D (2019) Bias correction of daily precipitation over South Korea from the long-term reanalysis using a composite gamma-pareto distribution approach. Hydrol Res 50(4):1138–1161. https://doi.org/10.2166/nh.2019.127

Kim YO, Lee JK (2010) Addressing heterogeneities in climate change studies for water resources in Korea. Curr Sci 98(8):1077–1083

Koutsoyiannis D (2004) Statistics of extremes and estimation of extreme rainfall: I. Theoretical investigation. Hydrol Sci J 49(4):575–590. https://doi.org/10.1623/hysj.49.4.575.54430

Koutsoyiannis D, Onof C (2001) Rainfall disaggregation using adjusting procedures on a Poisson cluster model. J Hydrol 246(1–4):109–122. https://doi.org/10.1016/S0022-1694(01)00363-8

Krishnan R, Sanjay J, Gnanaseelan C, Mujumdar M, Kulkarni A, Chakraborty S (2020) Assessment of climate change over the Indian region: a report of the ministry of earth sciences (MOES), government of India. In: Assessment of Climate Change over the Indian Region: a Report of the Ministry of Earth Sciences (MoES), Government of India. https://doi.org/10.1007/978-981-15-4327-2

Li SY, Miao LJ, Jiang ZH, Wang GJ, Gnyawali KR, Zhang J, Zhang H, Fang K, He Y, Li C (2020) Projected drought conditions in Northwest China with CMIP6 models under combined SSPs and RCPs for 2015–2099. Adv Clim Chang Res 11(3):210–217. https://doi.org/10.1016/j.accre.2020.09.003

Lima CHR, Kwon HH, Kim YT (2018) A local-regional scaling-invariant Bayesian GEV model for estimating rainfall IDF curves in a future climate. J Hydrol 566(August):73–88. https://doi.org/10.1016/j.jhydrol.2018.08.075
Liu K, Wang M, Zhou T (2021) Increasing costs to Chinese railway infrastructure by extreme precipitation in a warmer world. Transp Res Part d: Transp Environ 93(March):102797. https://doi.org/10.1016/j.trd.2021.102797
Lu LH, Stedinger JR (1992) Variance of 2-parameter and 3-parameter Gev Pwm quantile estimators - formulas, confidence-intervals, and a comparison. J Hydrol 138(1–2):247–267
Mailhot A, Duchesne S, Caya D, Talbot G (2007) Assessment of future change in intensity-duration-frequency (IDF) curves for Southern Quebec using the Canadian Regional Climate Model (CRCM). J Hydrol 347(1–2):197–210. https://doi.org/10.1016/j.jhydrol.2007.09.019
Maity R, Suman M, Laux P, Kunstmann H (2019) Bias correction of zero-inflated RCM precipitation fields: a copula-based scheme for both mean and extreme conditions. J Hydrometeorol 20(4):595–611. https://doi.org/10.1175/JHM-D-18-0126.1
Massey FJ (1951) The Kolmogorov-Smirnov test for goodness of fit. J Am Stat Assoc 46(253):68–78. https://doi.org/10.1080/01621459.1951.10500769
Mearns LO, Sain S, Leung LR, Bukovsky MS, McGinnis S, Biner S, Caya D, Arritt RW, Gutowski W, Takle E, Snyder M, Jones RG, Nunes AMB, Tucker S, Herzmann D, McDaniel L, Sloan L (2013) Climate change projections of the North American Regional Climate Change Assessment Program (NARCCAP). Clim Change 120(4):965–975. https://doi.org/10.1007/s10584-013-0831-3
Mishra V, Bhatia U, Tiwari AD (2020) Bias-corrected climate projections for South Asia from Coupled Model Intercomparison Project-6. Scientific Data 7(1):1–13. https://doi.org/10.1038/s41597-020-00681-1
Mishra V, Shah HL (2018) Hydroclimatological Perspective of the Kerala Flood of 2018. J Geol Soc India 92(5):645–650. https://doi.org/10.1007/s12594-018-1079-3
Molnar P, Burlando P (2005) Preservation of rainfall properties in stochastic disaggregation by a simple random cascade model. Atmos Res 77(1–4 SPEC. ISS.):137–151. https://doi.org/10.1016/j.atmosres.2004.10.024
Pai DS, Sridhar L, Rajeevan M, Sreejith OP, Satbhai NS, Mukhopadhyay B (2014) Development of a new high spatial resolution (0.25° × 0.25°) long period (1901–2010) daily gridded rainfall data set over India and its comparison with existing data sets over the region. Mausam 65(1):1–18
Papalexiou SM, Koutsoyiannis D (2013) Battle of extreme value distributions: a global survey on extreme daily rainfall. Water Resour Res 49(1):187–201. https://doi.org/10.1029/2012WR012557
Pavelsky TM, Sobolowsk S, Kapnick SB, Barnes JB (2012) Changes in orographic precipitation patterns caused by a shift from snow to rain. Geophys Res Lett 39(17):1–6. https://doi.org/10.1029/2012GL052741
Peck A, Prodanovic P, Simonovic SP (2012) Rainfall intensity duration frequency curves under climate change: City of London, Ontario, Canada. Canadian Water Resour J 37(3):177–189. https://doi.org/10.4296/cwrj2011-935
Pierce DW, Cayan DR, Maurer EP, Abatzoglou JT, Hegewisch KC (2015) Improved bias correction techniques for hydrological simulations of climate change. J Hydrometeorol 16(6):2421–2442. https://doi.org/10.1175/JHM-D-14-0236.1
Poonam RN, Rana N, Champati Ray PK, Bisht P, Bagri DS, Wasson RJ, Sundriyal Y (2017) Identification of landslide-prone zones in the geomorphically and climatically sensitive Mandakini valley, (central Himalaya), for disaster governance using the Weights of Evidence method. Geomorphology 284(June 2013):41–52. https://doi.org/10.1016/j.geomorph.2016.11.008
Rani SI, Arulalan A, George JP, Rajagopal EN, Renshaw R, Maycock A, Barker DM, Rajeevan M (2021) IMDAA: High resolution satellite-era reanalysis for the indian monsoon region. J Clim 1–78. https://doi.org/10.1175/jcli-d-20-0412.1
Ray K, Pandey P, Pandey C, Dimri AP, Kishore K (2019) On the recent floods in India. Curr Sci 117(2):204–218. https://doi.org/10.18520/cs/v117/i2/204-218
Riahi K, van Vuuren DP, Kriegler E, Edmonds J, O'Neill BC, Fujimori S, Bauer N, Calvin K, Dellink R, Fricko O, Lutz W, Popp A, Cuaresma JC, Samir KC, Leimbach M, Jiang L, Kram T, Rao S, Emmerling J, Tavoni M (2017) The Shared Socioeconomic Pathways and their energy, land use, and greenhouse gas emissions implications: an overview. Glob Environ Chang 42:153–168. https://doi.org/10.1016/j.gloenvcha.2016.05.009
Ring C, Pollinger F, Kaspar-Ott I, Hertig E, Jacobeit J, Paeth H (2018) A comparison of metrics for assessing state-of-the-art climate models and implications for probabilistic projections of climate change. Clim Dyn 50(5–6):2087–2106. https://doi.org/10.1007/s00382-017-3737-3
Ritschel C, Ulbrich U, Névir P, Rust HW (2017) Precipitation extremes on multiple timescales - Bartlett-Lewis rectangular pulse model and intensity-duration-frequency curves. Hydrol Earth Syst Sci 21(12):6501–6517. https://doi.org/10.5194/hess-21-6501-2017

Rojas R, Feyen L, Dosio A, Bavera D (2011) Improving pan-European hydrological simulation of extreme events through statistical bias correction of RCM-driven climate simulations. Hydrol Earth Syst Sci 15(8):2599–2620. https://doi.org/10.5194/hess-15-2599-2011

Roy SS, Balling RC (2004) Trends in extreme daily precipitation indices in India. Int J Climatol 24(4):457–466. https://doi.org/10.1002/joc.995

Schoetter R, Cattiaux J, Douville H (2015) Changes of western European heat wave characteristics projected by the CMIP5 ensemble. Clim Dyn 45(5–6):1601–1616. https://doi.org/10.1007/s00382-014-2434-8

Semmler T, Jacob D (2004) Modeling extreme precipitation events - a climate change simulation for Europe. Glob Planet Change 44(1–4):119–127. https://doi.org/10.1016/j.gloplacha.2004.06.008

Şen O, Kahya E (2021) Impacts of climate change on intensity–duration–frequency curves in the rainiest city (Rize) of Turkey. Theoret Appl Climatol 1017–1030. https://doi.org/10.1007/s00704-021-03592-2

Shin JY, Lee T, Park T, Kim S (2019) Bias correction of RCM outputs using mixture distributions under multiple extreme weather influences. Theoret Appl Climatol 137(1–2):201–216. https://doi.org/10.1007/s00704-018-2585-3

Shrestha A, Babel MS, Weesakul S, Vojinovic Z (2017) Developing Intensity-Duration-Frequency (IDF) curves under climate change uncertainty: the case of Bangkok, Thailand. Water (Switzerland) 9(2). https://doi.org/10.3390/w9020145

Shukor MSA, Yusop Z, Yusof F, Sa'adi Z, Alias NE (2020) Detecting rainfall trend and development of future Intensity Duration Frequency (IDF) curve for the State of Kelantan. Water Resour Manage 34(10):3165–3182. https://doi.org/10.1007/s11269-020-02602-8

Singh R, Arya DS, Taxak AK, Vojinovic Z (2016) Potential impact of climate change on rainfall intensity-duration-frequency curves in Roorkee, India. Water Resour Manage 30(13):4603–4616. https://doi.org/10.1007/s11269-016-1441-4

Singh T, Saha U, Prasad VS, Gupta MD (2021) Assessment of newly-developed high resolution reanalyses (IMDAA, NGFS and ERA5) against rainfall observations for Indian region. Atmos Res 259(May):105679. https://doi.org/10.1016/j.atmosres.2021.105679

Srivastav RK, Schardong A, Simonovic SP (2014) Equidistance quantile matching method for updating IDFCurves under climate change. Water Resour Manage 28(9):2539–2562. https://doi.org/10.1007/s11269-014-0626-y

Sun Q, Zhang X, Zwiers F, Westra S, Alexander LV (2021) A global, continental, and regional analysis of changes in extreme precipitation. J Clim 34(1):243–258. https://doi.org/10.1175/JCLI-D-19-0892.1

Tegegne G, Kim YO, Lee JK (2019) Spatiotemporal reliability ensemble averaging of multimodel simulations. Geophys Res Lett 46(21):12321–12330. https://doi.org/10.1029/2019GL083053

Watt WE, Waters D, McLean R (2003) Climate change and urban stormwater infrastructure in Canada: Context and case studies. Toronto-Niagara Region study report and working paper deries, Waterloo, Ontario. Report 2003–1, p 27

Yeo MH, Van Nguyen VT, Kpodonu TA (2021) Characterizing extreme rainfalls and constructing confidence intervals for IDF curves using Scaling-GEV distribution model. Int J Climatol 41(1):456–468. https://doi.org/10.1002/joc.6631

Yu PS, Yang TC, Lin CS (2004) Regional rainfall intensity formulas based on scaling property of rainfall. J Hydrol 295(1–4):108–123. https://doi.org/10.1016/j.jhydrol.2004.03.003

Publisher's Note Springer Nature remains neutral with regard to jurisdictional claims in published maps and institutional affiliations.